

Shear Stress in Magnetorheological Finishing for Glasses

Introduction

Magnetorheological finishing (MRF) is a sub-aperture polishing tool for fabrication of precision optics. The removal function of MRF is based on a magnetorheological (MR) fluid that consists of magnetic carbonyl iron (CI), non-magnetic polishing abrasives, and water or other non-aqueous carrier fluids and stabilizers. The MR fluid ribbon stiffens in the presence of a magnetic field to form a localized polisher, and spindle-mounted parts are moved through the polishing zone to polish the surface and to correct the figure.^{1,2}

For conventional polishing processes, the material removal rate (MRR, $\Delta h/\Delta t$ where Δh is a representative height of removal averaged over the entire part area) is predicted by the traditional Preston relationship or Preston's equation:³

$$\text{MRR} = C_p P V = C_p \frac{F_n}{A_c} V, \quad (1)$$

where C_p is the Preston coefficient, which includes the effects of the process parameters affecting the interaction between the work piece and the tool (e.g., pH, slurry, type of abrasives, frictional forces, etc.), P is the normal pressure applied (i.e., normal force F_n divided by the contact area A_c between the polishing tool/pad and the substrate being polished), and V is the relative velocity between the part and the tool. The applicability of Preston's equation for material removal in MRF is a subject of study. Shorey⁴ used the spot-taking machine (STM, described in detail on p. 44) to measure drag force on a sapphire part, using a drag force measuring device and aqueous MR fluids consisting of different types and concentrations of CI particles and abrasives. Shorey⁴ found that there is a strong positive linear relationship between the material removal rate for sapphire and the drag force in MRF, predicting a similar result for fused silica (FS), although drag force values under the above conditions were not reported for FS. Shorey also calculated that the normal force acting on a single abrasive particle (within the MR fluid ribbon) and the part is approximately 1×10^{-7} N (Ref. 4). This is several orders of magnitude

smaller than that for conventional polishing, 5 to 200×10^{-3} N (Ref. 5). Shorey concluded that there must be drag force to have removal in MRF.

To address MRF, first Kordonski⁶ and later Shorey⁴ proposed a modified Preston's coefficient $C'_{p,\text{MRF}}(F_n)$ in terms of the normal force F_n by introducing a coefficient of friction (COF, μ), correlating material removal rate for MRF (MRR_{MRF} , identified as $\Delta h/\Delta t$, where Δh is a representative height of removal averaged over the MRF spot area) with drag force. Equation (2) shows this transition as described by Shorey:

$$\begin{aligned} \text{MRR}_{\text{MRF}} &= C'_{p,\text{MRF}}(F_n) \frac{\mu F_n}{A_s} V = C'_{p,\text{MRF}}(F_d) \frac{F_d}{A_s} V \\ &= C'_{p,\text{MRF}}(\tau) \times \tau \times V, \end{aligned} \quad (2)$$

where, for MRF, the normal force F_n is divided by the spot area A_s , instead of A_c [Eq. (1)]. A_s is the projected spot area over which polishing occurs (see **Characterization**, p. 46), i.e., the pressure applied by the hydrodynamic flow of MR fluid at the gap between the part surface and the STM wheel.⁷ $C'_{p,\text{MRF}}(F_d)$ is a modified Preston's coefficient for MRF in terms of drag force. The drag force F_d divided by the spot area A_s equals the shear stress τ . $C'_{p,\text{MRF}}(\tau)$ is a modified Preston's coefficient in terms of shear stress [note that $C'_{p,\text{MRF}}(\tau) = C'_{p,\text{MRF}}(F_d)$]. Equation (2) predicts that material removal in MRF is proportional to the hydrodynamic pressure and shear stress. Although they did not report on shear stress, Shorey⁴ and Shorey *et al.*⁸ indicated that the normal force in MRF is relatively small compared to conventional polishing techniques, and therefore, material removal in MRF is governed by shear stress rather than the hydrostatic pressure. It is also important to note that this is the first time where the modified Preston's coefficient, as suggested by Kordonski⁶ and Shorey,⁴ is associated with respect to either normal force or drag force/shear stress.

DeGroot⁹ incorporated Shorey's⁴ modified Preston equation, specifically the proportionality between material removal

rate and shear stress, in an empirical model for characterizing MRF of optical glasses with nanodiamonds. Using a drag force sensor other than Shorey's,⁴ DeGroot studied six optical glasses: three phosphates and three silicates. DeGroot⁹ and DeGroot *et al.*¹⁰ found that the peak removal rate (assuming a constant contact zone for all materials divided by the spotting time) increased (silicates) or decreased (phosphates) linearly with drag force. Drag force and peak removal rate did not show the same linear correlation across all six optical glasses since "chemistry and glass composition play a significant role in the MRF material removal process, and removal rate cannot be characterized by drag force alone."¹⁰ It is also important to note that because the spot area was assumed to be constant for all glasses, drag force and shear stress were considered to be equivalent (within a constant of proportionality) when discussing the relationship between these two properties and material removal.

Using the same drag force sensor as DeGroot,⁹ Miao *et al.*¹¹ calculated shear stress from MRF drag force measurements for a variety of materials including optical glasses, polycrystalline ceramics, and hard metals and found a positive linear dependence of peak removal rate with shear stress. They did not consider, however, how shear stress is correlated to material properties.

As reviewed above, previous work concentrated only on the contribution of drag force to material removal in MRF. Limited study was carried out on shear stress that is closely related to drag force, but incorporates the MRF spot area A_s . This article reports on the use of a dual force sensor for the real-time, simultaneous measurement of both drag force and normal force in MRF. We study how the measurable normal and drag forces, and calculated shear stress with respect to the measured projected spot area on the part surface, contribute to material removal in MRF for optical glasses based on

their mechanical properties. The variability of the value for the Preston's coefficient in MRF over the three glass types is examined in terms of the normal force, drag force, shear stress, and a material figure of merit. We propose a new modification to the Preston's equation that predicts MRF material removal rate in terms of mechanical properties and shear stress for optical glasses.

The following sections (1) describe materials tested in this work, the STM experimental platform, data acquisition, and methodology used for characterizing experimental results; (2) present MRF spotting results including spot depth, area and volume, removal rate, and force measurement data; (3) discuss the dependence of drag and normal forces on material properties, the role of shear stress in MRF material removal, and the modified Preston's equation; and (4) present conclusions based on this work.

Experimental Details

1. Materials

Three types of optical glasses were chosen for this study based on their economic importance: phosphate (LHG8), borosilicate (BK7), and fused silica (FS). LHG8 is a phosphate laser glass that is widely used in high-peak-power laser systems. It is mechanically soft and has moderate chemical durability. BK7 and FS are optical glasses commonly used for visible and ultraviolet applications because of their excellent chemical, mechanical, and optical properties. The materials' mechanical properties, ranked in order by increasing Vickers hardness, are listed in Table 117.I. The figure of merit (FOM) shown in Table 117.I is defined as $E/K_c H_V^2$, where E is Young's modulus (resistance to elastic deformation), H_V is Vickers hardness (resistance to plastic deformation), and K_c is fracture toughness (resistance to fracture/crack growth). This figure of merit was originally used by Lambropoulos *et al.*¹² to evaluate volumetric removal in loose-abrasive lapping of optical glasses.

Table 117.I: Physical and mechanical properties of optical glasses rank in order by increasing Vickers hardness.^(a)

Material	Mat. ID	Young's Modulus E (GPa)	Vickers Hardness H_V (GPa)	Fracture Toughness ^(b) K_c (MPa \times m ^{1/2})	Figure of Merit ^(c) $E/K_c H_V^2$ ($\times 10^{-3}$ MPa ⁻² \times m ^{-1/2})	Source
Phosphate	LHG8	62	3.7	0.5	8.71	Hoya
Borosilicate	BK7	81	6.0	0.8	2.81	Schott
Fused Silica	FS	69	7.5	0.8	1.64	Corning

^(a)Mechanical properties are from Ref. 9 where glass hardness was measured using a 100-gf load; errors for all values are less than $\pm 25\%$.

^(b)Fracture toughness numbers were calculated using the model of Evans.¹³

^(c)Figures of merit (FOM) were calculated after Lambropoulos *et al.*¹²

The relationship between the FOM and the removal rate in MRF is discussed on p. 47.

Three pieces of each material were used in this work, except LHG8, for which only one piece was available. All substrates were flats, pitch polished in LLE's Optical Fabrication Shop to a surface flatness of less than $1 \mu\text{m}$ for all materials¹⁴ and to a root-mean-square (rms) surface roughness of less than $\sim 2 \text{ nm}$ (Ref. 15). All substrates were round disks ($\sim 40 \text{ mm}$) with thicknesses varying from $\sim 2 \text{ mm}$ to $\sim 10 \text{ mm}$.

2. Spot-Taking Machine

An MRF spot-taking machine (STM, see Fig. 117.41) was used as a test bed to take removal-rate data in the form of spots on part surfaces *without part rotation*. Unlike a commercial MRF machine, the STM has only z -axis motion and cannot be used to polish a surface. The MRF removal function from the STM is characterized with an MRF spot that is created by lowering a nonrotating part into the rotating MR fluid ribbon. Material is removed in a characteristic D-shaped spot, as shown in Fig. 117.42.

The STM operating settings were kept constant for all spots taken in this work. Fluid temperature was held at $\sim 23^\circ\text{C}$. The mixing rate within the fluid confinement vessel was 1000 rpm,

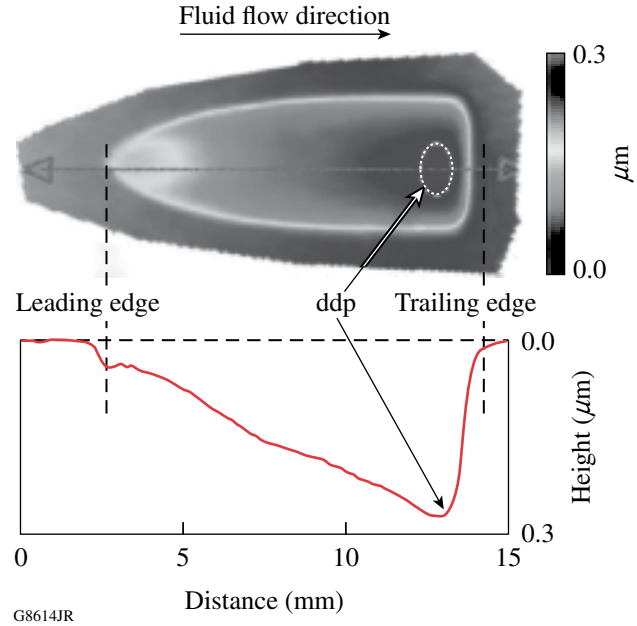


Figure 117.42 Interferometric image of an MRF spot on BK7 glass and its accompanying profile.¹⁴ The dashed ellipse denotes the depth-of-deepest-penetration (ddp) region where a maximum amount of material is removed. Parallel dashed lines indicate the leading edge (where the MRF ribbon starts to contact the part) and the trailing edge (where the MRF fluid ribbon leaves the part). The MR fluid is flowing from left to right. The spot line profile is extracted through the center of the spot image; the distance from the leading edge to the trailing edge is $\sim 12 \text{ mm}$ and the spot depth is $\sim 0.28 \mu\text{m}$.

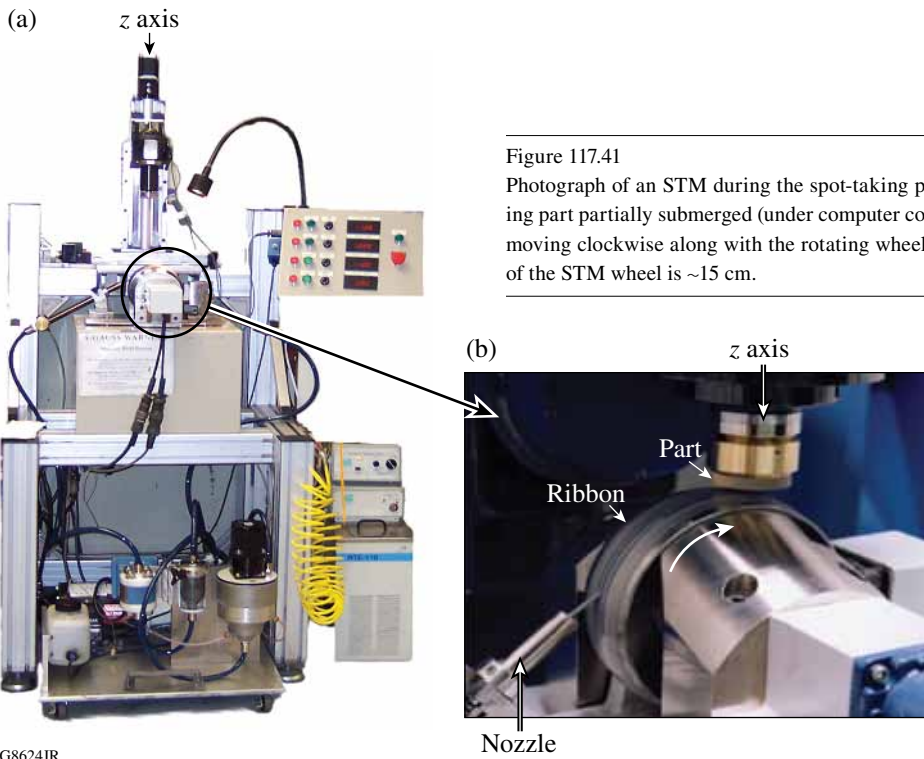


Figure 117.41 Photograph of an STM during the spot-taking process: (a) spot-taking machine; (b) the nonrotating part partially submerged (under computer control) into the stiffened MR fluid ribbon, which is moving clockwise along with the rotating wheel. The STM has only z -axis motion. The diameter of the STM wheel is $\sim 15 \text{ cm}$.

the magnetic pole-piece current was 15 A (resulting in a magnetic field strength of 2 to 3 kG), the wheel speed was 200 rpm, and the out-of-field viscosity was 45 cP, as measured on the STM. The pump speed was adjusted to maintain a ribbon height of 1.6 mm, and the depth of the part immersed into the MR fluid ribbon, precisely controlled by computer, was kept constant at 0.3 mm. Spotting times (i.e., dwell times) varied from 1.17 s to 2.16 s in order to keep spot depths within the measurement range of a laser interferometer (see **Characterization**, p. 46).

A standard aqueous magnetorheological (MR) fluid was used in this experiment. This MR fluid consisted of carbonyl iron (CI) particles, nonmagnetic nanodiamond abrasives, deionized (DI) water, and stabilizers. The CI particles used in the MR fluid had a median particle size of $\sim 4 \mu\text{m}$. A small amount of nanodiamond particles, $\sim 50\text{-nm}$ median size,⁹ were used as polishing abrasives to enhance the material removal efficiency.

3. Dual-Force Sensor/Sample Mounting Device

A mounting device was developed for measuring both drag and normal forces acting on the part surface during MRF spotting, as shown in Fig. 117.43. The device consists of two dynamic piezoelectric force sensors,^{16,17} mounted directly above the MR fluid ribbon and part surface contact zone. This ensures that both the sensors and the part align along the machine's z axis. This configuration limits the spotting experiment to one spot per part, except for LHG8 where only one part was available, requiring a small offset of the part

itself. The sample mount portion of the device was modified to permit this adjustment.

The sensors are suitable for measuring relatively low forces (response threshold less than 0.1 and 0.01 N for the drag and normal force sensors, respectively),^{16,17} which makes it possible to detect subtle changes in substrate type and surface condition, MR fluid composition, and STM machine settings. Special care was taken to keep the part's surface horizontal and perpendicular to the z axis for force measurements during spotting. System noise encountered in previous mounts was overcome by fabricating the force sensor/sample mounting device from aluminum to reduce its overall weight and by installing two 150-Hz filters (hardware) on both dual-mode amplifiers used for data acquisition.

Off-line calibration of the dual-force sensor assembly was performed on each material individually after each part was mounted. The normal-force sensor and drag-force sensor were calibrated separately. The calibration test showed that the vertical load applied for calibrating the normal-force sensor did not introduce a horizontal-force signal in the drag-force sensor, and a horizontal force applied for calibrating the drag-force sensor did not introduce a vertical-force signal in the normal-force sensor.

A LabVIEW interface was designed to record drag- and normal-force signals simultaneously.¹⁸ Force was averaged over the spotting time for each individual measurement.

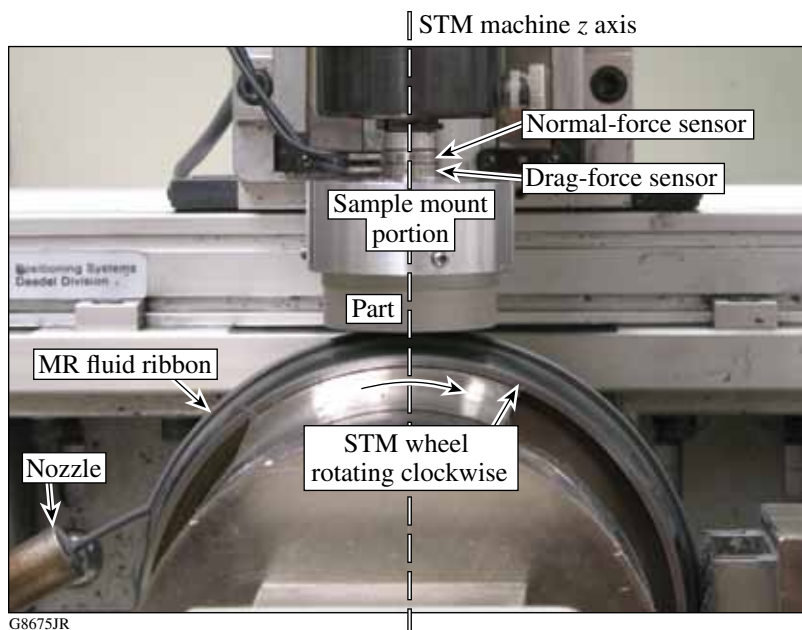


Figure 117.43

Photograph of the dual force sensor/sample mounting device, during spot taking on the STM, indicating the machine's z axis, the normal- and drag-force sensors, the sample mounting device, a part, the MR fluid ribbon, and the rotating wheel (diameter ~ 15 cm). The sensors are located directly above the contact zone between the MR fluid ribbon and the part for real-time *in-situ* measurements. The sample is waxed to a glass disk held by a set of screws against the aluminum housing of the sample mounting device.

4. Characterization

Removal rates for parts were obtained from MRF spots. The initial surface flatness was determined by a Zygo Mark IVxp interferometer (HeNe Fizeau interferometer),¹⁴ which was also used to determine MRF-spot physical properties including spot profile, depth of deepest penetration (ddp), spot area, and spot volume. Spot volume (the volume of material removed in the spot) was measured using the laser interferometer by subtracting the original surface (before spotting) from the new surface that included the spot.¹⁹ Volumetric removal rate was calculated as the spot volume divided by the spotting time. Spot area A_s was obtained by “drawing” a contour line on the spot periphery (light outline seen in the image in Fig. 117.42). Pressure was calculated by dividing normal force by spot area. Shear stress was calculated by dividing drag force by spot area.

It is important to note that in MRF, the contact area A_c and the spot area A_s are not the same. A_c represents the whole area of the part in contact with the MR fluid ribbon, while A_s is where the material removal effectively takes place during MRF spotting. The spot area, within the contact area, is normally slightly smaller, due to the fact that shear stress at the spot edge is almost zero, resulting in negligible material removal. Results from spotting experiments (not described here) demonstrate that A_c is the same for all materials when spotted under the same STM settings; A_s is, however, dependent on material type.

The peak-to-valley (p-v) and root-mean-square (rms) surface roughness within the spot ddp region for all materials was measured with a Zygo NewView 5000 noncontacting

white-light interferometer.¹⁵ Unfiltered areal ($350 \times 260 \mu\text{m}^2$) surface roughness data were acquired at five randomly located sites within the spot ddp region for every spot taken.

Experimental Results

All spotting experiments were conducted under the same STM settings (except for the spotting time described in **Spot-Taking Machine**, p. 44) within a three-day period, approximately ten days after loading the MR fluid into the STM. Table 117.II summarizes the experimental results, including spot ddp, calculated peak removal rate ($\Delta h/\Delta t$), area (projected spot area), volume, calculated volumetric removal rate (VRR), drag force (F_d), normal force (F_n), and p-v and rms surface roughness. The rate of material removal is given in terms of volumetric removal rate. VRR is a practical measure of process efficiency providing a three-dimensional representation of material removal over the whole spot area (notice that the horizontal scale of Fig. 117.42 is in millimeters, whereas the vertical line, i.e., the spot depth, is in micrometers). Surface roughness data entered in Table 117.II for each material are averaged over 15 measurements, taken at five sites within the ddp region of each of three spots.

Drag force (F_d) is between ~ 4 to ~ 5 N, and normal force is between ~ 6 to ~ 9 N. These results fall within the range (2 to 20 N) of normal-force values reported by Schinhaerl *et al.*²⁰ using a three-axis dynamometer and a cerium-oxide MR fluid on BK7 glass over a range of operating conditions. Figure 117.44 plots both normal and drag forces versus the materials' Vickers hardness, where it is seen that only normal force has a positive linear dependence on material hardness.

Table 117.II: Experimental data for materials after spotting.

Material	Spotting time (s)	ddp (μm)	Peak removal rate ($\mu\text{m}/\text{min}$)	Spot area (mm^2)	Spot volume ($\times 10^6 \text{mm}^3$)	Volumetric removal rate (mm^3/min)	F_d (N)	F_n (N)	p-v (nm)	rms (nm)
LHG8	1.17	0.9 ± 0.014	46 ± 0.8	36 ± 2	10.1 ± 0.7	0.517 ± 0.038	4.0 ± 0.0	6.2 ± 0.4	12 ± 2	1.5 ± 0.2
BK7	1.17	0.28 ± 0.001	14 ± 0.1	54 ± 1	5.4 ± 0.2	0.268 ± 0.016	5.1 ± 0.1	8.4 ± 0.2	14 ± 1	1.6 ± 0.3
FS	2.16	0.28 ± 0.016	8 ± 0.4	50 ± 0.1	3.4 ± 0.1	0.102 ± 0.012	4.1 ± 0.1	9.3 ± 0.3	9 ± 1	1.0 ± 0.1

Material	F_d/F_n	F_n/A_s (MPa)	F_d/A_s (MPa)
LH8	0.64 ± 0.04	0.17 ± 0.0157	0.11 ± 0.0001
BK7	0.61 ± 0.01	0.16 ± 0.0052	0.09 ± 0.00126
FS	0.44 ± 0.01	0.19 ± 0.0085	0.08 ± 0.0028

The measured ratio of drag force to normal force (F_d/F_n) falls between ~ 0.4 to ~ 0.6 , which is in the typical range for the coefficient of friction (COF) reported for most materials in the sliding friction mode.²¹ This is the first reported measurement of F_d/F_n for MRF.

The resultant p-v and rms surface roughness after the spotting process is expected since the sample piece is not rotated. These areal rms values of ~ 1 nm are typical of those previously reported for glass spotted on the STM.⁸⁻¹⁰

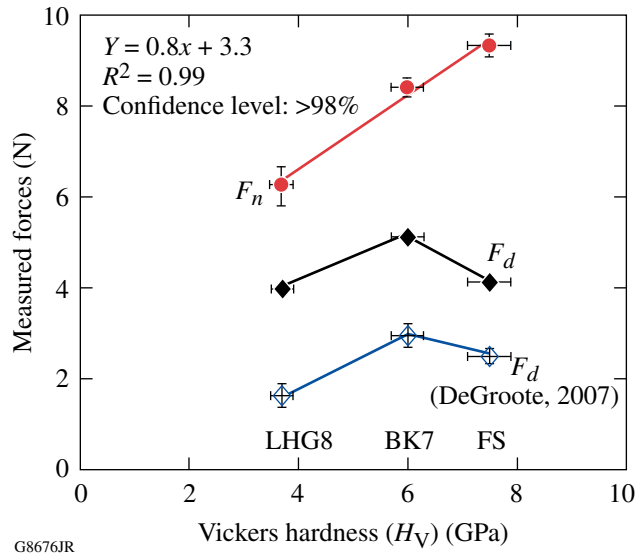


Figure 117.44
Normal force F_n and drag force F_d as a function of the material's Vickers hardness (GPa) for LHG8, BK7, and FS. (See text for a discussion of data taken by DeGroote.⁹)

Discussion

1. From Normal Force to Hydrodynamic Pressure, from Drag Force to Shear Stress

For the first time, both drag force (F_d) and normal force (F_n) are measured simultaneously *in situ* for MRF. This section discusses how these measured forces correspond to the material removal model presented in the **Introduction** (p. 42) and its validity to MRF.

Normal force shows a positive linear dependence on material type (Fig. 117.44) under the conditions used in this experiment. Broadly speaking, material wear depends on its mechanical hardness, i.e., a soft material will wear more rapidly than a harder one. Our results show that the normal force is sensitive to the substrate surface hardness and, therefore, must have some, as yet undetermined, role to play in the motion/interaction between the MR fluid ribbon and the part.

In addition, the volumetric removal rate decreases as normal force increases, as seen from the data in Table 117.II. However, when an attempt is made to plot and examine (not shown here) the ratio of F_n/A_s , i.e., the hydrodynamic pressure, to material Vickers hardness, no dependence is seen. Likewise, plotting the volumetric removal rate versus the hydrodynamic pressure (not shown here) reveals no dependence. (Note that the calculated hydrodynamic pressure range is from 0.1 to 0.3 MPa. This is comparable to literature values for pressure found in conventional chemical mechanical polishing processes.²²) These results confirm experimentally that hydrodynamic pressure has negligible effect on material removal, and, contrary to previous reports,⁴ the normal force is affected by the material hardness. The next section evaluates the different process parameters that affect the removal rate in MRF.

Figure 117.44 shows that the drag force alone does not depend on material type. This was originally reported by DeGroote⁹ (see Fig. 117.44) on the STM, using a different force-sensor mounting device that included only a drag-force sensor. The current results are $\sim 100\%$, 20% , and 60% higher for LHG8, BK7, and FS, respectively, compared to those measured previously. This increase in the measured drag force is attributed to improved alignment of the location of the drag-force sensor relative to the STM z axis and different MRF fluid/spotting conditions; otherwise, the results are similar.

It is not clear why drag force does not show an upward or downward trend with material hardness. As suggested by DeGroote⁹ and DeGroote *et al.*,¹⁰ the contribution of the glass-surface chemical dissolution to material removal in the MRF process is not explicitly represented by any terms in Eq. (2). The effect of chemistry on lowering the drag force experienced by the phosphate LHG8 could be considerable. A modification of Eq. (2) is offered in the next section, which provides a relatively simple prediction of material removal for MRF from that described by DeGroote⁹ and DeGroote *et al.*,¹⁰ without considering chemical contributions in the removal process.

Our results indicate that the hydrodynamic flow pressure in the converging gap, between the workpiece and MR fluid ribbon, depends on the composition of the upper gap surface. If pure no-slip boundary conditions held at the part surface, one would expect both normal and drag (shear) forces to be independent of part composition. We conclude, therefore, that the no-slip boundary condition must be violated to some extent on the part's surface. This is not surprising, given the fact that the MR fluid consists of a high concentration of solid abrasives in an aqueous medium.

Figure 117.45 plots the volumetric removal rate as a function of shear stress, F_d/A_s . It shows a strong dependence between material removal and shear stress, as predicted by Eq. (2), for shear stress values between ~ 0.08 to 0.15 MPa for the three glasses under the specific conditions of this experiment. It can also be extrapolated from these results that, for shear stresses less than about 0.08 MPa, the removal rate practically vanishes. This suggests a shear stress threshold below which material removal is very low; therefore the process efficiency is very low. As seen from Fig. 117.45, the volumetric removal rate does not depend on the hydrodynamic pressure F_n/A_s .

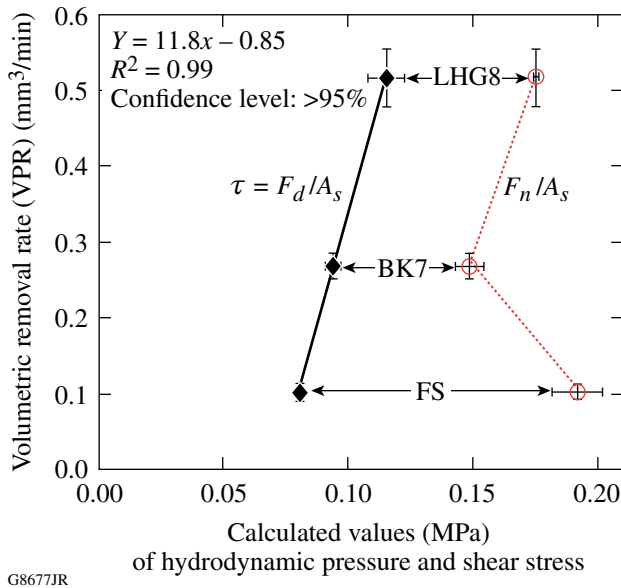


Figure 117.45
Volumetric removal rate (VRR) as a function of shear stress (τ), F_d/A_s , and as a function of the hydrodynamic pressure F_n/A_s .

2. Material Removal Rate Model

Lambropoulos *et al.*²³ found that the material removal rate is linearly proportional to both material mechanical properties (combined into a mechanical FOM) and pressure for loose-abrasive lapping of optical glasses. Their equation is now modified to describe material removal in MRF on the basis of the mechanical contributions to a FOM. Vickers hardness (H_V) is used in this analysis instead of Knoop hardness (H_K). The exponents of the mechanical property components are simplified as $E/K_c H_V^2$ (this term is designated as the mechanical FOM), similar to DeGroot's⁹ and DeGroot *et al.*,¹⁰ where near-surface Young's modulus and nanohardness were used instead of bulk values.

We next discuss the development of a coefficient to describe MRF removal similar to $C'_{p,MRF}(\tau)$ in Eq. (2). To establish such a coefficient, we may use either pressure (as usually done in Preston analysis) or shear stress (as our current work indicates).

The effects of both shear stress (τ) and mechanical properties ($E/K_c H_V^2$) can be incorporated into a predictive equation for material removal as shown in Eq. (3):

$$\text{MRR}_{\text{MRF}} = C'_{p,MRF}(\tau, \text{FOM}) \frac{E}{K_c H_V^2} \times \tau \times V, \quad (3)$$

where $C'_{p,MRF}(\tau)$ is a modification of Preston's coefficient in terms of shear stress τ and the material FOM. MRR_{MRF} could alternatively be written as the ratio $\text{VRR}_{\text{MRF}}/A_s$, which is identified as $\Delta h/\Delta t$, where VRR_{MRF} is the volumetric removal rate for MRF and Δh is a representative height of removal averaged over the whole spot area.

For a linear velocity ~ 1.57 m/s at the wheel edge, assuming that the nanodiamond abrasives and the CI particles in the stiffened MR fluid ribbon are moving at the same speed as the rotating wheel, it is possible to estimate values for each of the three Preston's coefficients identified in Eqs. (2) and (3). Table 117.III shows the calculated values for $C'_{p,MRF}(F_n)$, $C'_{p,MRF}(\tau)$, and $C'_{p,MRF}(\tau, \text{FOM})$ for all materials spotted by MRF along with literature values for C_p from conventional loose-abrasive polishing on a polyurethane pad. The coefficients are calculated from $\text{VRR}_{\text{MRF}}/A_s$, as discussed above. The calculated $C'_{p,MRF}(F_n)$ varies from as low as 1.2×10^{-4} GPa⁻¹ for FS to as high as 8.8×10^{-4} GPa⁻¹ for LHG8, nearly an 8 \times increase. $C'_{p,MRF}(\tau)$ has a smaller range, however, of about 5 \times , from 2.6×10^{-4} GPa⁻¹ for FS to 1.4×10^{-3} GPa⁻¹ for LHG8. Substituting shear stress for pressure narrows the range of Preston's coefficient; however, because of the absence of material properties, there is still a significant variance in $C'_{p,MRF}(\tau)$. Combining shear stress with mechanical properties results in a much tighter range of the coefficient $C'_{p,MRF}(\tau, \text{FOM})$ from 1.6×10^{-4} GPa⁻¹ for FS up to 2.0×10^{-4} GPa⁻¹ for BK7, only a single variance in magnitude. The coefficient $C'_{p,MRF}(\tau, \text{FOM})$ varies by only $\pm 12\%$ among LHG8, BK7, and FS, which may be attributable to the particular surface condition and specific material composition.

Table 117.III: Preston's coefficient for conventional chemical mechanical polishing processes from literature and modified Preston's coefficients calculated for MRF from this work.

Material	C_p (GPa ⁻¹)	$C'_{p,MRF}(F_n)$ (GPa ⁻¹)	$C'_{p,MRF}(\tau)$ (GPa ⁻¹)	$C'_{p,MRF}(\tau, FOM)$ (MPa)
LHG8	–	8.8×10^{-4}	1.4×10^{-3}	1.6×10^{-4}
BK7	8.3×10^{-4} (a) 10.7×10^{-4} (b)	3.4×10^{-4}	5.6×10^{-4}	2.0×10^{-4}
FS	1.7×10^{-4} (a) 3.3×10^{-4} (b)	1.2×10^{-4}	2.6×10^{-4}	1.6×10^{-4}
Variance in magnitude ^(c)	–	8×	5×	≪1×

^(a)From Izumitani,^{24,25} using conventional loose-abrasive lapping, CeO₂ abrasives and polyurethane pad, $p = 20$ KPa, $V = 0.5$ m/s.

^(b)From Cumbo,²⁶ using conventional loose-abrasive lapping, CeO₂ abrasives and polyurethane pad, $p = 5$ KPa, $V = 0.11$ m/s.

^(c)Variance in magnitude is defined by dividing the largest value in the column by the smallest value.

Conclusions

This work reports for the first time on *in-situ* measurements of drag and normal forces in MRF. Three optical glasses ranging in hardness and chemical composition were tested. A spot-taking machine (STM) was used as a test bed for MRF spotting experiments. We examined how the measurable drag and normal forces, and the calculated shear stress as a function of material mechanical properties, contribute to material removal in MRF. A modified Preston's equation, combining shear stress with material mechanical properties, is proposed, which suggests that material removal is dominated by the material mechanical properties. Our main observations are summarized as follows:

- Normal force was measured simultaneously with drag force in MRF for the first time. Normal force was within the range of 6 to 9 N, whereas drag force was within the range of 4 to 5 N. These results are in good agreement with the literature, where either one of these forces was measured individually, but not simultaneously.
- It was confirmed experimentally that the hydrostatic pressure [normal force divided by the projected spot area F_n/A_s , first term of Eq. (1) (see data in Table 117.II and Fig. 117.45)] does not predict the material removal rate in MRF. It was found for the first time that the measured normal force is dependent on material hardness.
- It was also demonstrated for the first time how the calculated shear stress (drag force divided by the projected spot area on

the part) governs the volumetric removal rate, not drag force alone. This experimentally confirms Shorey's⁴ predictions that material removal in MRF is dominated by shear.

- For the glasses tested under the STM geometry and conditions reported here, it was found that there is a threshold for shear stress below which a removal rate becomes negligible. In order to effectively remove material in MRF, shear stress should be kept above ~ 0.08 MPa by adjusting the process parameters. Additional work is required to identify what process parameters affect shear stress, such as the size of the projected spot area on the part. Our results show that drag force is within a range of ~ 4 to 5 N for a range of optical glass materials, ranging from relatively "soft" LHG8 to hard FS. Therefore, by keeping a spot area < 50 mm² while keeping drag force in the range reported above, one should expect efficient material removal in MRF for glasses.
- Preston's coefficient was calculated for MRF in terms of the hydrostatic pressure, shear stress, and a combination of a material's figures of merit and shear stress. These calculated coefficients indicate a narrow range for our modified Preston's coefficient when both material figures of merit and shear stress are considered for a range of optical glasses, providing predictive capabilities for new glasses. Therefore, we conclude that material removal in MRF for optical glasses is governed by a material's mechanical properties and shear stress.

ACKNOWLEDGMENT

The authors thank Alex Maltsev and Mike Kaplun of the Laboratory for Laser Energetics (LLE) for their help with sample preparation. The authors also thank Scott Russell of the Department of Mechanical Engineering at the University of Rochester for his help with the LabVIEW software. The authors acknowledge the Laboratory for Laser Energetics (LLE) at the University of Rochester for continuing support. One of the authors (C. Miao) is an LLE Horton Fellow.

Research was sponsored by the U. S. Army Armament, Research, Development and Engineering Center (ARDEC) and was accomplished under Cooperative Agreement Number W15QKN-06-2-0104 and the U.S. Department of Energy Office of Inertial Confinement Fusion under Cooperative Agreement No. DE-FC52-08NA28302, the University of Rochester, and the New York State Energy Research and Development Authority. The views and conclusions contained in this document are those of the authors and should not be interpreted as representing the official policies, either expressed or implied, of U.S. Army ARDEC or the U.S. Government. The support of DOE does not constitute an endorsement by DOE of the views expressed in this article. The U.S. Government is authorized to reproduce and distribute reprints for Government purposes notwithstanding any copyright notation hereon.

REFERENCES

1. S. D. Jacobs, D. Golini, Y. Hsu, B. E. Puchebner, D. Strafford, Wm. I. Kordonski, I. V. Prokhorov, E. Fess, D. Pietrowski, and V. W. Kordonski, in *Optical Fabrication and Testing*, edited by T. Kasai (SPIE, Bellingham, WA, 1995), Vol. 2576, pp. 372–382.
2. S. D. Jacobs, S. R. Arrasmith, I. A. Kozhinova, L. L. Gregg, A. B. Shorey, H. J. Romanofsky, D. Golini, W. I. Kordonski, P. Dumas, and S. Hogan, in *Finishing of Advanced Ceramics and Glasses*, edited by R. Sabia, V. A. Greenhut, and C. G. Pantano, Ceramic Transactions, Vol. 102 (The American Ceramic Society, Westerville, OH, 1999), pp. 185–199.
3. F. W. Preston, *J. Soc. Glass Technol.* **XI**, 214 (1927).
4. A. B. Shorey, “Mechanisms of Material Removal in Magnetorheological Finishing (MRF) of Glass,” Ph.D. thesis, University of Rochester, 2000.
5. V. H. Bulsara *et al.*, *Trans. ASME, J. Appl. Mech.* **65**, 410 (1998).
6. V. W. Kordonski and D. Golini, in *Proceedings of the Sixth International Conference on Electro-Rheological Fluids, Magneto-Rheological Suspensions and Their Applications*, edited by M. Nakano and K. Koyama (World Scientific, Singapore, 1998), pp. 837–844.
7. D. Golini, H. Pollicove, G. Platt, S. Jacobs, and W. Kordonski, *Laser Focus World* **31**, 83 (1995).
8. A. B. Shorey, S. D. Jacobs, W. I. Kordonski, and R. F. Gans, *Appl. Opt.* **40**, 20 (2001).
9. J. E. DeGroot, “Surface Interactions Between Nanodiamonds and Glass in Magnetorheological Finishing (MRF),” Ph.D. thesis, University of Rochester, 2007.
10. J. E. DeGroot, A. E. Marino, J. P. Wilson, A. L. Bishop, J. C. Lambropoulos, and S. D. Jacobs, *Appl. Opt.* **46**, 7927 (2007).
11. C. Miao, S. N. Shafir, H. Romanofsky, J. Mici, J. C. Lambropoulos, and S. D. Jacobs, in *Optical Fabrication and Testing*, OSA Technical Digest (CD) (Optical Society of America, Washington, DC, 2008), Paper OTThB4.
12. J. C. Lambropoulos, S. D. Jacobs, and J. Ruckman, in *Finishing of Advanced Ceramics and Glasses*, edited by R. Sabia, V. A. Greenhut, and C. G. Pantano, Ceramic Transactions, Vol. 102 (The American Ceramic Society, Westerville, OH, 1999), pp. 113–128.
13. A. G. Evans, in *Fracture Mechanics Applied to Brittle Materials*, edited by S. W. Freiman (American Society for Testing and Materials, Philadelphia, 1979), Vol. ASTM STP 678, Part 2, pp. 112–135.
14. Zygo Mark IVxp™, Zygo Corporation, Middlefield, CT 06455. This instrument is a 4-in. HeNe Fizeau interferometer with a wavelength of 632.8 nm. Peak-to-valley (p–v) for surface flatness and depth of deepest penetration (ddp) of the spot was measured in microns.
15. Zygo NewView 5000 noncontact white light interferometer, Zygo Corporation, Middlefield, CT 06455. Average microroughness data (peak-to-valley, p–v, and root-mean-square, rms) were obtained under the following conditions: 20× Mirau objective; high FDA Res.; 20- μ m bipolar scan length; Min/Mod: 5%, unfiltered. This instrument has a lateral resolution of $\sim 1 \mu\text{m}$ and a vertical resolution of $\sim 0.3 \text{ nm}$.
16. Single-axis slim-line compressive (K9133B21) force sensor measuring system, Kistler Instrument Corp., Amherst, NY 14228-2171.
17. Single-axis slim-line shear (K9143B21) force sensor measuring system, Kistler Instrument Corp., Amherst, NY 14228-2171.
18. The LabVIEW data-collecting program (National Instruments Corporation, Austin, TX 78759-3504) was written by S. Russell and S. N. Shafir of the University of Rochester, Rochester, NY (2008).
19. MetroPro Reference Guide, OMP-0347, Zygo Corporation, Middlefield, CT 06455.
20. M. Schinhaerl *et al.*, in *Current Developments in Lens Design and Optical Engineering IX*, edited by P. Z. Mouroulis, W. J. Smith, and R. B. Johnson (SPIE, Bellingham, WA, 2008), Vol. 7060, p. 706006.
21. B. Bhushan and B. K. Gupta, in *Handbook of Tribology: Materials, Coatings, and Surface Treatments* (Krieger Publishing Company, Malabar, FL, 1997), Chap. 2, Table 2.1, p. 2.11.
22. J. Steigerwald, S. P. Murarka, and R. J. Gutmann, *Chemical Mechanical Planarization of Microelectronic Materials* (Wiley, New York, 1997).
23. J. C. Lambropoulos, S. Xu, and T. Fang, *Appl. Opt.* **36**, 1501 (1997).
24. T. S. Izumitani, in *Optical Fabrication and Testing*, OSA Technical Digest (Optical Society of America, Washington, DC, 1982), pp. 1–4.
25. T. S. Izumitani, in *Optical Fabrication and Testing Workshop*, OSA Technical Digest (Optical Society of America, Washington, DC, 1984), pp. TuB-A1-1–TuB-A1-3.
26. M. J. Cumbo, “Chemo-Mechanical Interactions in Optical Polishing (Glass Finishing),” Ph.D. thesis, University of Rochester, 1993.